Master's Thesis of Engineering

Micro-miniaturized Neural Recording Motes using Mid-field wireless Energy Transfer for Implantable Brain Machine Interface

이식형 뇌-기계 접속을 위한 중거리 무선 전력 전송 시스템과 이를 이용한 신경 측정 미세 임플란트 개발

August 2016

Graduate School of Convergence Science and Technology
Seoul National University

Program in Nano Science and Technology

Jihun Lee

Micro-miniaturized Neural Recording Motes using Mid-field wireless Energy Transfer for Implantable Brain Machine Interface

Yoon-Kyu Song

Submitting a master's thesis of
Engineering

August 2016

Graduate School of Convergence Science and Technology
Seoul National University

Program in Nano Science and Technology
Jihun Lee
August 2016

Chair	**Youn Sang Kim**	**(seal)**
Vice Chair	**Yoon-Kyu Song**	**(seal)**
Examiner	**Chang Soon Kim**	**(seal)**

Abstract

Micro-miniaturized Neural Recording Motes using Mid-field wireless Energy Transfer for Implantable Brain Machine Interface

Jihun Lee

Program in Nano Science and Technology

The Graduate School

Seoul National University

Invasive Brain-Machine Interface(BMI) has revealed the high potential to assist motor or communication functions of patients with paralysis or neurological impairment. However, most of the system requires maintained transcutaneous wiring between recording electrodes and external devices, which raises the risks of infection and limits the range

of behavior of subjects. Thus, many research teams have tried to develop wireless neural implant with an internal battery or external power transmission strategies. Nevertheless, a number of safety problems still remain unsolved due to a large footprint of implant, heat generation and limited power supply.

Herein, to address those challenges, we developed the micro-miniaturized neural recording sensors by combining Mid-field Wireless Power Transfer and RFID(Radio-Frequency Identification) technique. Mid-field Wireless Power Transfer is a recently suggested method that realizes optimal current density to create energy-focused region deep in biological tissue allowing the receiving coil to be made extremely small. By using an electromagnetic structural simulator, we designed Mid-field WPT antenna that can approximate optimal current density with single-phase source. This antenna also operates at a dual frequency (2.46 GHz and 4.92 GHz) realizing high efficiency both in wireless powering and backscattered signal readout. On the top of that, we designed neural implant as passive RFID sensor consisted by commercial electronic components, such as Schottky diode and RF bipolar junction transistor(BJT). The Schottky diode generates harmonic component of received source power and RF BJT performs highly nonlinear mixing of RF carrier and amplified neural potentials. All components are compactly bonded together small enough to be inserted inside 2mm diameter coil and the overall implant was encapsulated in

epoxy resin.

Performance test of the powering system and the neural implant was conducted at multi-layer agar phantom simulating relative permittivity and electrical conductance of skin, skull, dura and gray matter, white matter. In this measurement, our wireless powering system achieves a transmission efficiency of 3.3×10^{-3} for 2.46 GHz and 4.6×10^{-4} for 4.92 GHz when the miniature coil is placed in target separation, 17.5mm. This powering system allows the recording sensor to have a remarkably small footprint (3 mm × 5 mm), which is only 6% of a comparable system. With this micro-miniaturized footprint, our implant is theoretically able to monitor the extracellular potential as low as 47 μV_{pp} from a high impedance electrode (20 Kohm). Our system demonstrated its ability to extract neural signals while minimizing potential trauma or physiological interference from the implant. Further improvement of this study will pave the way for a broad range of clinical application of wireless BMI from hospital to daily life.

Keywords: Brain-Machine-Interface, Mid-field wireless energy transfer, wireless neural implant, Radio Frequency IDentification

Student Number : 2014-24817

Table of Contents

List of figures

efficiency between dual-band mid-field antenna and a 2-mm diameter coil as a function of separation distance at 2.46 GHz and 4.92 GHz.

Figure 7 (a) Measured spectral response of a neural motes system to emulated neural signals (2 mVpp at 1 kHz). (b) System loss as a function of neural signal frequency.

Figure 8 System loss as a function of neural signal frequency. (c) An example of input signals and recovered waveforms of sinusoid wave (left) and extracellular potential (right). The arbitrary function generator with 20 Kohm source impedance produced input signals of 1mVpp at 1kHz.

Figure 9 The input extracellular potential waveform (up) and the recovered signals (down) superimposed in a 4 ms window.

Figure 10 The result of SAR measurement (a) Temperature rise of phantom as a function of RF radiation exposure duration. (b) Spatial SAR1g distribution measured using thermographic method.

Chapter 1. Introduction

1.1. Conventional brain-machine interface

The Brain Machine Interface (BMI) is a one of the major neuroscience methods that can record neural activities and decode them to extract information or intention encoded in brain signals, such as action potential, electroencephalogram(EEG) or electrocochleography. It has revealed the potential as a clinical method by decoding brain signals of impaired patient to control external devices, such as a wheelchair, computer cursor, a speech synthesizer, or neural prosthetics [1]. Among this signal recording system, invasive BMI systems utilizing intracortical Multi-Electrode Array (MEA) showed promising recording results with a high level of temporal and spatial resolution in preliminary human trials and non-human primate test [2-4]. For instance, by using the system that use a 96-channel microelectrode array to record signals from motor cortex, woman who were tetraplegic and anarthric was able to control robitc arm only with thoughts [2]. However, most of these systems require maintained opening on the skin and cortical bone due to the percutaneous connection between recording units and external devices. This connection raises the risks of infection and limits the range of behavior of subjects, which cause physical and psychological burden on patients. Therefore, these system has been applied only for severely disabled patients who have any other channel

for commucation, such as people with tetraplegia or amyotrophic lateral sclerosis. Also, the maintenance of system requires the stringent supervision of medical professionals in controled circumstance [5, 6]. For these reasons, it has been a major challenge to develop fully wireless BMI system in the field of neural engineering not only to do research on the brain activity of freely moving subjects but also to establish a clinical BMI system for daily use.

1.2. Wireless active neural implant

With a battery and/or wireless powering methods, a few leading research groups already developed BMI implants using an Integrated Circuit (IC) for multi-channel neural signal processing. This neural processing circuit consist of a low-power amplifier, a bandpass filter, an analog multiplexer, an analog-to-digital converter, a digital controller, and data telemetry [7-10]. With this implant, it was possible to record multi-channel neural signals, up to hundreds of channels, wirelessly from the cortex of non-human primates [11-13]. However, some safety-related problems remain unsolved. Due to the lifetime of battery, regular battery replacement surgery is required for several implants. Also, the implantation of battery inside head has potential risks of explosion or electrolyte leakage, which can endanger the life of patient. Additionally, most system has a large footprint up to 5 cm due to complex signal processing circuit and wireless power receiver.[11-13] Implant with this size not only can disturb the natural physiology of

brain but also can damage patient with a severe brain contortion. On the top of that, these active circuit consume high energy inside patient's head, which can cause an irreversible brain damage from heat dissipation. [14-16].

1.3. Wireless passive neural implant

As an alternative brain implant, RFID-based neural tags or passive neural implants with a mixer circuit have been proposed while minimizing active signal processing on a circuit to reduce negative influences of an implant [17-21]. Nevertheless, currently available neural sensors still suffer from a trade-off relationship between a receiver size and an operation depth. This is because conventional wireless powering methods, such as inductive coupling or radiative energy transfer, are not suitable for powering receiver inside the dispersive biological tissue [22-24]. Particularly, when the size of the receiver is millimeter-scale, an effective power transmission distance declines rapidly. In addition, most of the neural RFID and passive mixer circuit have low conversion efficiency and/or low input impedance [19, 25]. However, in vivo recording condition, neural potentials rarely exceed a millivolt while recording electrodes tend to show a high impedance (~Kohms) at an interface between the electrode and the tissue [26-28].

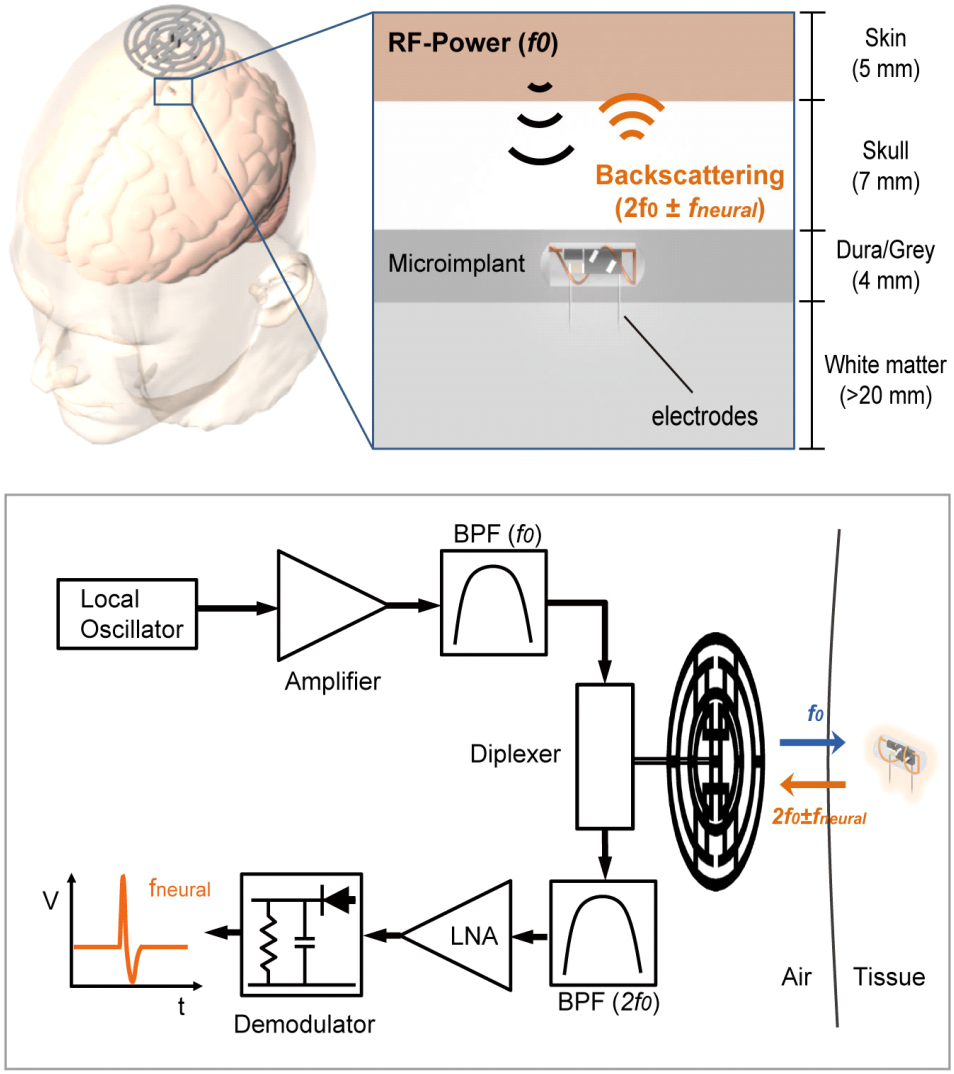

Figure 1 Schematics of the neural recording motes system featuring a passive neural sensor and external interrogator for wireless powering (2.46 GHz) and backscattered signal reading (4.92 GHz).

Here, we present a safe and reliable neural recording system with a micro-miniaturized size and an in-vivo recording ability. By using a mid-field wireless energy transfer strategy suggested recently, we developed a novel dual-band antenna that can establish a highly efficient power and data link with a miniature coil receiver (2mm inner diameter) inside the multi-layer tissue. Also, a RFID neural circuit with a high input impedance and detection sensitivity was designed to extract neural signals from high impedance electrodes. As integrating these components, our neural implant exhibits a significantly smaller footprint, less than 6% of a comparable implant [19, 25], while achieving high conversion efficiency, up to 17 dB, from a neural signal (fneural) to backscattered signal (4.92 GHz ± fneural). Due to these characteristics, neural motes system can theoretically detect neural potentials as low as 47 μVpp causing a minimal brain damage and physiological interference. This recording ability shows that our mote system has a high potential as an experimental or clinical method available in the laboratory, the hospital or even daily life.

Chapter 2. Design and experiments

The neural mote system in this study has three major components: a dual-band midfield antenna for wireless power transmission and backscatter reading, a highly sensitive radio frequency identification (RFID) node that amplifies the neural potential signals and mixes them with a carrier to backscatter 4.92GHz ± f_{neural}, and an external interrogator with an RF (radio frequency) power source and a neural signal recovery block.

2.1. Theory and design of dual band mid-field antenna

To achieve high energy transmission efficiency in the midfield region, we adopted an optimization methodology suggested by a research team at Stanford University. In this analysis, the power transfer efficiency is determined by the coupling factor (γ), which is the ratio of the power harvested at the coil to the total absorbed power in tissue [29]. When assuming a small coil receiver of area A_r and length l_r with self-impedance R_r, the coupling efficiency γ can be expressed as

$$\gamma = \frac{\left| i\omega\mu_0 A_r \mathrm{H}(\mathrm{r}_r)\cdot\hat{\alpha} + l_r \mathrm{E}(r_r)\cdot\hat{\beta}\right|^2}{\omega R_r \int \mathrm{Im}\,\epsilon(r)\left|\mathrm{E}(\mathrm{r})\right|^2 d\mathrm{r}} \quad (1)$$

where the vectors $\hat{\alpha}$ and $\hat{\beta}$ denote the orientations of the magnetic

and the electric dipoles, respectively, with the volume integral in the denominator extending to all tissue layers. In this equation, H(r) and E(r) correspondingly represent the magnetic field and the electric field from the transmitting source, and the location r_r is where the receiver is implanted. Using the dyadic Green's functions, this equation can be expressed as a function of the source current density *Js*. Doing so enables solving for the optimal source current density *Js* to maximize the coupling factor (γ) for a magnetic and electric dipole. These current density levels create a high energy density region deeply inside the multi-layer biological tissue, allowing the energy-harvesting receiver to be extremely small [30, 31]. Using this analysis, in MATLAB, the 2D current density that maximizes the power efficiency between the antenna and the coil receiver was solved as a vector space structure at a dual frequency (2.46/4.92 GHz).

To realize the optimal coupling factor, we designed a unique two-layer antenna that generates a major current flow of the optimal current density by means of electromagnetic simulation. This antenna can approximate the optimal current for an electric dipole only with a single-phase source and create the characteristic field propagation of the midfield wireless transfer process (see Fig. 2). Furthermore, antennas intended to operate at two different frequencies were integrated to achieve dual-band emission as a wireless power source (2.46 GHz) and for backscatter reader (4.92 GHz ± f_{neural}).Two-layer metal plates were fabricated separately by laser machining and soldered together to simplify the structure. The receiver was designed as acoil with an inner

diameter of 2 mm and a length of 5 mm and was manually fabricated with 200um copper wire insulated with polyamide approximately 20 μm thick. The impedance of the coil was matched with the recording circuit in at the dual-band frequency to facilitate both the harvesting of 2.46 GHz and the backscattering of 4.92 GHz signals.

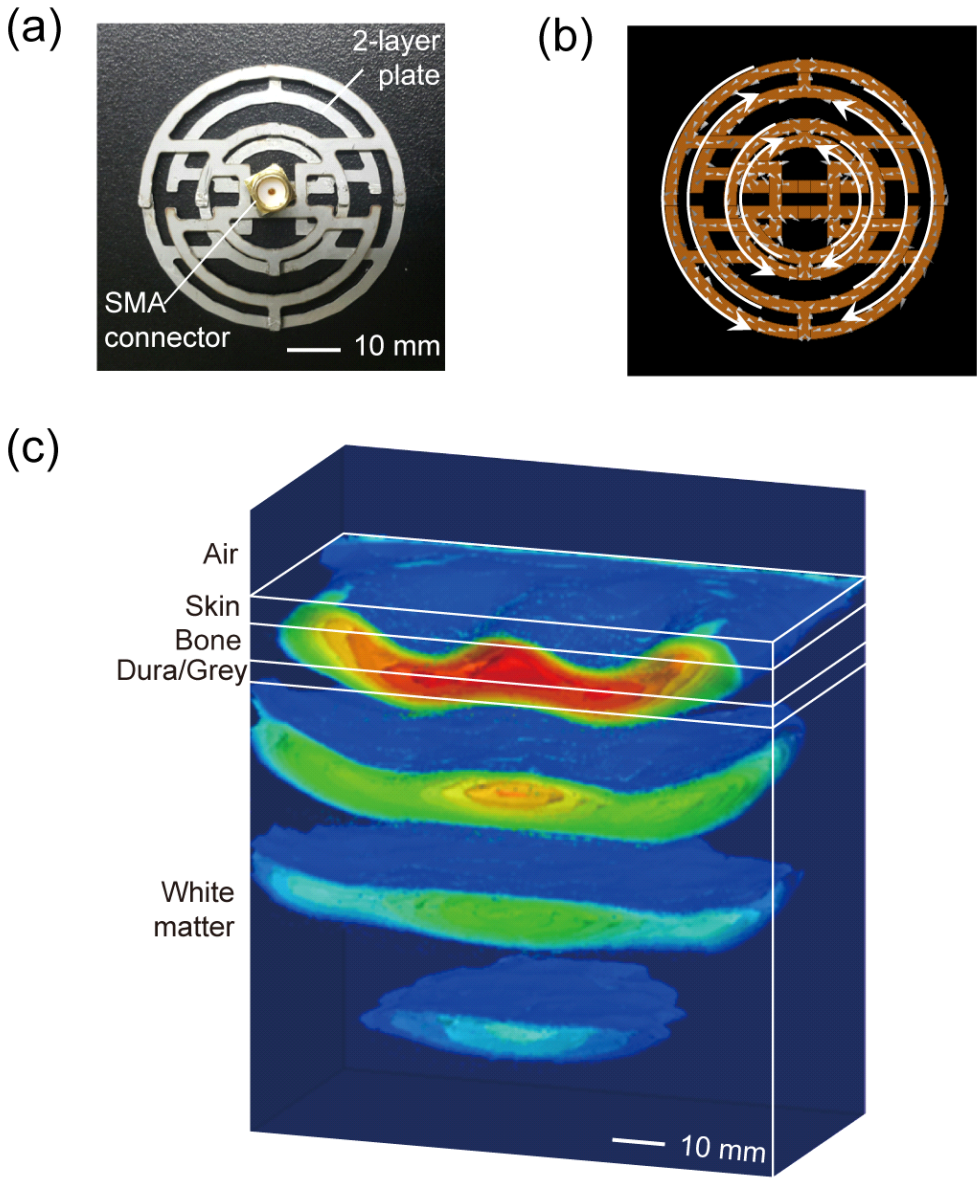

Figure 2 Design and operation of the proposed dual band mid-field antenna. (a) The fabricated two-layer metal plate antenna with SMA connector. (b) The current density of antenna (arrow head) and the optimal current density (white arrow) at 2.46 GHz. The scale of current density was express by the color of arrow head. (c) The generated electric field component aligned with the receiver electric dipole.

2.2. Theory and design of neural recording motes

The RFID neural circuit was designed to perform frequency doubling, amplification and backscattering modulation with a minimal number of circuit elements. This circuit consists of two major components, a frequency doubler and an amplifying mixer. As a frequency doubler, a low-barrier Schottky diode, SMS-7630, generates a second-order harmonic product (4.92 GHz) of the carrier signal (2.46 GHz) to isolate backscattering signals from the reflected waves. In addition, this diode imposes directional properties in the circuit, which simplifies the forward biasing circuit for the following transistor.

In a common RFID mixer, a field effect transistor (FET) generates the backscattering signal because the change in the drain-source current (I_{ds}) accordingly modulates the impedance which arises across the coil terminals. The modulation of I_{ds} is a function of the gate-source voltage (V_{gs}), which can range from 100 to 2000 μV_{pp}foranelectrodeinsertedintothebrain[9]. The detection sensitivity, S, to neural signals can be defined as the change in I_{ds} with regard to V_{gs} normalized by the nominal I_{ds} (in addition to the current-through biasing resistor R_{b1} and R_{b2}) and V_{neural},

$$S = \frac{V_{neural}}{I_{ds} + V_{ds} / \left(R_{b1} + R_{b2}\right)} \cdot \frac{\partial I_{ds}}{\partial V_{gs}}$$

$$= V_{neural} \cdot \frac{g_m}{I_{ds} + V_{ds} / \left(R_{b1} + R_{b2}\right)}$$

Given that g_m (the transconductance of the FET) is directly

proportional to I_{ds}, to maximize g_m/I_{ds} (i.e., to achieve the largest value of g_m for a given I_{ds}), the FET must operate in its deep sub-threshold region, where it acts as a bipolar junction transistor (BJT). In this condition, a BJT can be an alternative to maximize the detection sensitivity, as an ideal BJT can obtain an S value of 400 ppm when V_{neural}= 10 μV_{pp}[32]. Due to this high detection sensitivity, a mixer using a BJT operates as if it is an amplifier and a modulator at the same time. For this reason, we used an RF BJT, BFU-760F, to achieve high conversion efficiency from neural signals (f_{neural}) to the backscattering sideband (4.92 GHz ± f_{neural}) while increasing the input impedance of the circuit.

With these components, the circuit was designed as shown in Fig. 3. The conversion gain depending on the source impedance and the linearity over the neuropotential frequency range (100-5000 Hz) was verified in an RF circuit simulation. Each of the circuit components were compactly stacked and soldered together such that the overall circuit was small enough to be inserted inside a 2mm coil. This process not only minimizes the footprint of the implant but also reduces the influence of the line impedance in a high-frequency wave. The fabricated implant was encapsulated with an epoxy resin, and the size of the final product was about 3 mm ×5 mm on average.

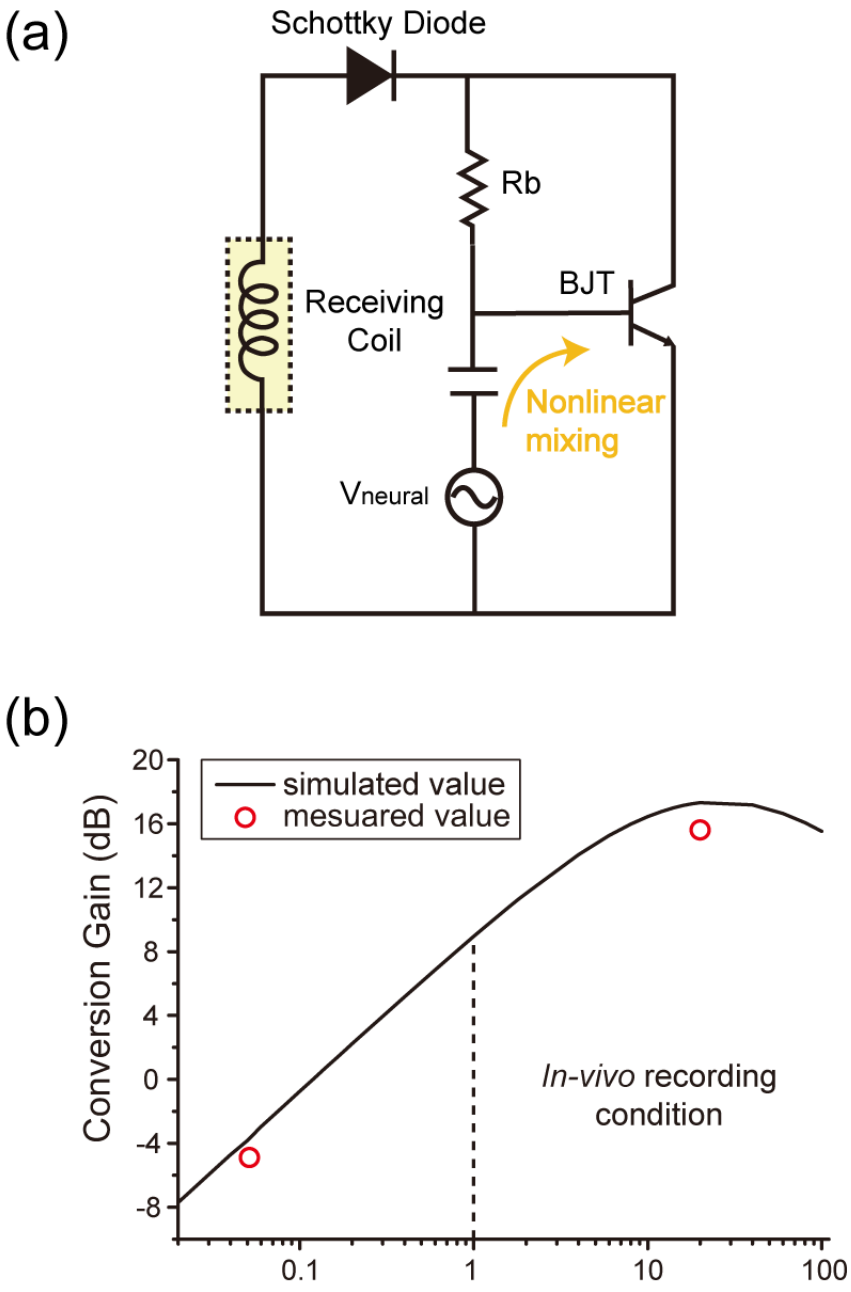

Figure 3 (a) The schematic for circuit design and operation, (b) The implant circuit's conversion gain from neural signals (f_{neural}) to backscattering signals (4.92 GHz ± f_{neural}) depending source Impedance.

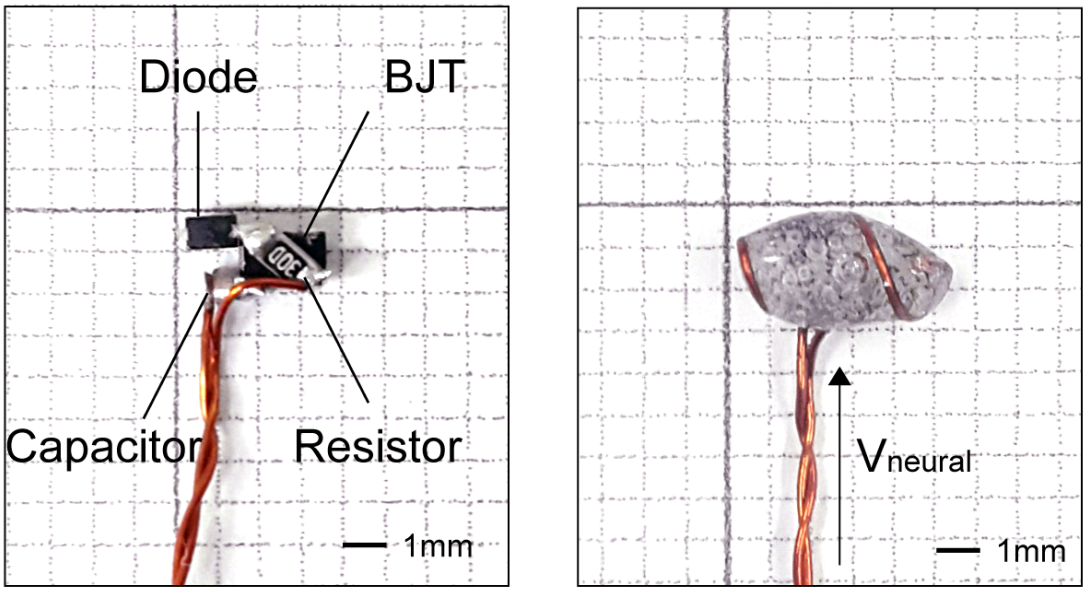

Figure 4 Stacked circuit components including bipolar junction transistor, schottky diode, capacitor and resistor (left) and the encapsulated overall implant (right)

2.3. Measurement setup

The overall performance of the antenna and the neural implant was evaluated within an agar phantom to simulate electromagnetic properties of biological tissue. The phantom formulas were adapted from earlier studies [19, 33], where the permittivity and conductivity of the phantom were adjusted using polyethylene powder and sodium chloride (NaCl), respectively. In a four-layer head phantom (skin 5mm, skull 7mm, dura and gray matter 4mm, and white matter >20mm), the mixture ratio was varied depending on the characteristics of each layer. The dura and gray matter layers were combined as one layer, as the electrical properties of the dura layer (<0.5 mm) are similar to those of gray matter.

First, the RF emission in a range of 2-5.5 GHz of our dual-band antenna was measured with a network analyzer, an Agilent E5071C. A homogeneous skin phantom was placed 5 mm away from the antenna to mimic an operation condition. After the verification of the antenna, the efficiency of the wireless power transfer from the antenna to the coil receiver was measured at both frequencies (2.46/4.92 GHz) at various separation distances. To simplify the experimental tests, the receiver was implanted into the homogeneous skin phantom because it can approximate a multilayer phantom with a minor difference only at 2.46 GHz, up to 3 dB. At the scale of a motes, standard electrical measurements can be misleading due to coupling with conductive

probes. Thus, we designed a rectifying circuit while closely approximates the matching condition of a neural implant circuit. By measuring the rectified DC voltage level of the rectifier implant, the power received from the coil at a specific implantation depth was evaluated.

Backscattering signals were analyzed to demonstrate the recording performance of the system. In this measurement, the neural recording mote was implanted inside the four-layer head phantom to mimic the operating environment as closely as possible. As shown in Fig. 1, the RF signal source generated a 2.46 GHz carrier signal (30 dBm) and fed it to the dual-band antenna through a diplexer. The neural recorder placed in the gray matter layer harvested the power from the antenna (17.5 mm separation, including a 5 mm air gap) and backscattered the third-order harmonic product (4.92 GHz ± f_{neural}). The external antenna then collected the backscattered signals and relayed them to a spectrum analyzer or a signal-recovery block via the diplexer. The signal-recovery block consisted of a bandpass filter (4.92GHz), multi-stage RF amplifiers (LNA-6G,RF-bay), an amplitude modulation (AM) demodulator and a neural processing integrated chip with an amplifier and a bandpass filter (100-5 kHz). In this stage, real-time neural signals (f_{neural}) were recovered from backscattered signals (4.92 GHz ± f_{neural}) using a demodulator and were then amplified before being displayed on an oscilloscope. An arbitrary waveform generator provided two types of emulated potentials, sine and extracellular potential waves at f_{neural} = 100 – 5000 Hz, to the neural implant through a wired connection. The

source impedance of the waveform generator was adjusted to 20 KOhms to emulate *in-vivo* recording conditions.

SAR is a measure of the rate at which human tissue absorbs electromagnetic energy. It can be measured with a thermographic method by observing the increase in the temperature induced by RF emission [34, 35]. The temperature elevation (ΔT) can be linearly correlated to the SAR as follows:

$$\mathrm{SAR} = C \left.\frac{\partial T}{\partial t}\right|_{t \to 0} = C \frac{\Delta T}{\Delta t} \tag{3}$$

In this equation, C [J/(kg·K)] is the specific heat of the sample and Δt (seconds) is the duration of exposure to radiation. When achieving a sufficient ΔT within a limited Δt (<60 seconds), thermal diffusion is negligible, and Equation (3) becomes valid [36]. In our SAR measurement, the dual-band midfield antenna radiated 1.58 W RF waves at 2.46 GHz for various durations. After the radiation exposure, the thermal increase of the cross-section of the four-layer phantom was measured by an FLIR-335 infrared (IR) camera. To normalize the infrared emissivity to ~ 0.95, a thin layer of black paint was sprayed onto exposed phantom halves [35]. Between each trial, the phantom was cooled to room temperature.

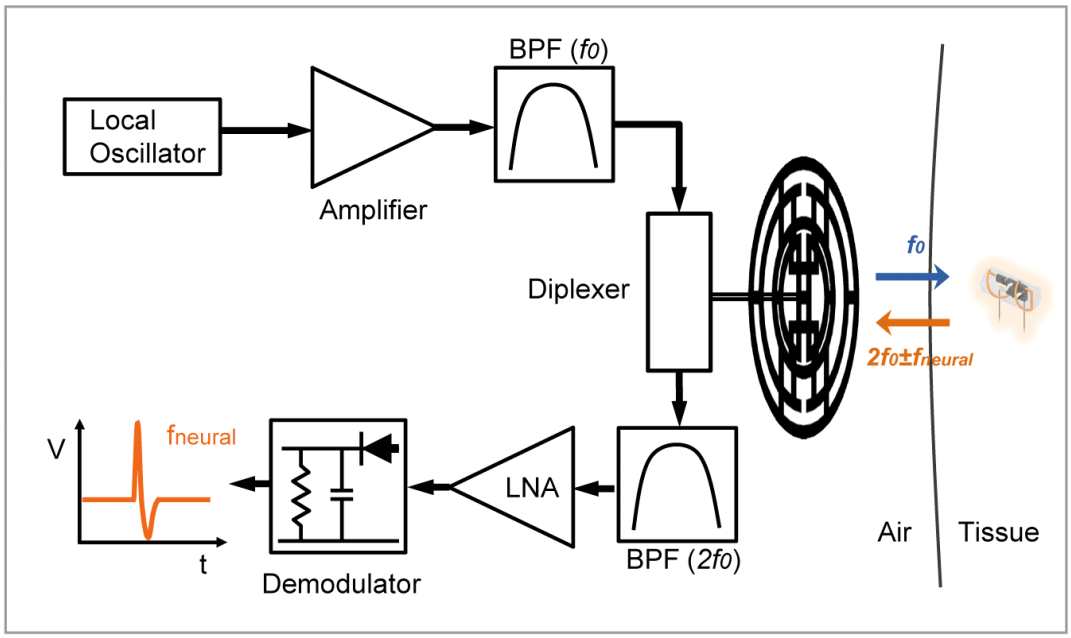

Figure 5 Block diagram of external interrogator with RF power source and signal recovery unit.

Chapter 3. Results and discussion

3.1. Antenna performance

In dual-band antenna test, the emission pattern of the antenna closely complied with the simulation result over 2-5.5 GHz, showing resonances at 2.46 GHz and 4.92 GHz. (see Fig. 5) This antenna achieved an efficiency of 3.3×10-3 for 2.46 GHz and 4.6×10-4 for 4.92 GHz at the target separation of 17.5 mm. As seen in Fig. 5(b), this result nearly approaches the simulation result, 1.5 dB higher for 2.46 GHz and 3.8 dB lower for 4.92GHz. These errors are likely due to discrepancies in phantom layer thickness and the mismatch loss between the coil and the circuit at high frequency. Due to the propagation character of midfield wireless powering, coil receiver even in deep brain area (>40 mm) can harvest power sufficient to operate a tiny medical device consuming about ten to hundreds of microwatts [38].

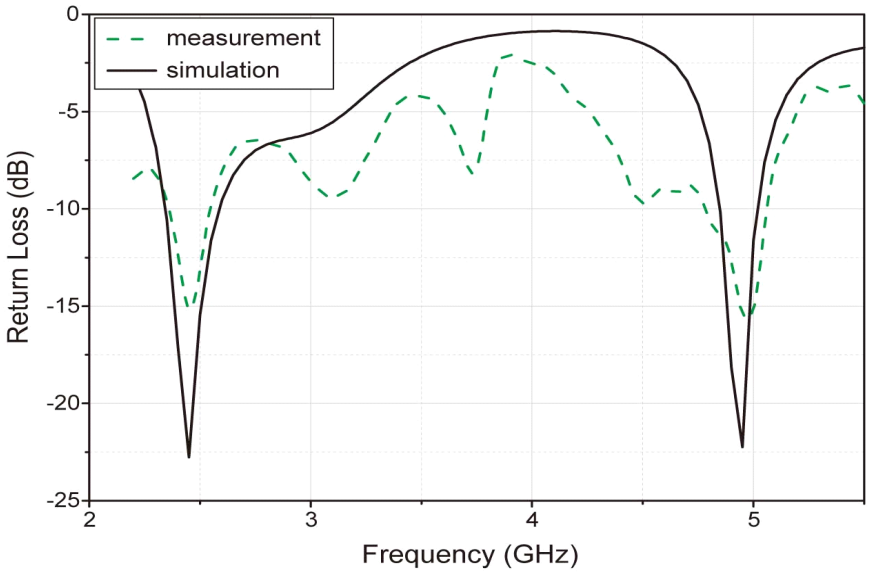

(a)

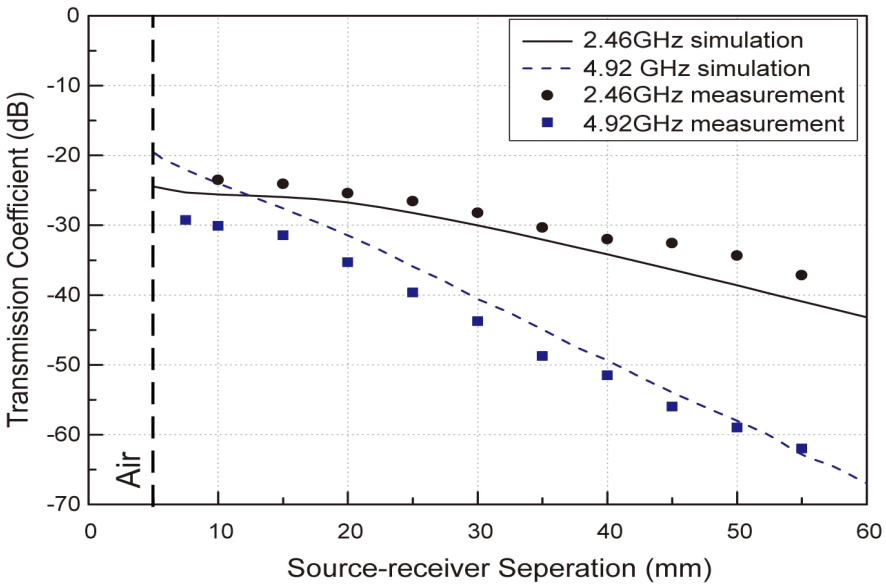

(b)

Figure 6 (a) Return loss of dual band mid-field antenna measured by network analyzer (b) Simulated, and measured transmission efficiency between dual-band mid-field antenna and a 2-mm diameter coil as a function of separation distance at 2.46 GHz and 4.92 GHz.

3.2. Frequency-domain performance

At the external interrogator, the backscattered signals were detected via a spectrum analyzer. A spectral response for emulated neural signal at 100-5000 Hz was measured (see Fig. 5). From measurement results, the system loss was calculated by subtracting the received sideband power level (4.92 GHz ± fneural) from the generated neural signal power (fneural). This System loss (Lsys) can be divided as

$$L_{sys}[\mathrm{dB}] = G_{conv}[\mathrm{dB}] + L_{trans}[\mathrm{dB}] + L_{mat}[\mathrm{dB}] \quad (4)$$

where Gconv is the conversion efficiency of the circuit from the neural signal (fneural) to backscattering sideband (4.92 GHz ± fneural), Ltrans is the transmission loss between the coil and antenna, and Lmat is the mismatch loss between the coil and the implant circuit [19]. As shown in Fig. 5. (b), the system loss of our implant was measured to be 21.5 dB and 42 dB when source impedance was 20 Kohms and 50 Ohms, respectively. This is 5.5 dB higher than simulation results likely due to the large mismatch loss Lmat between the coil and the circuit. Notably, unlike the other RFID neural recording devices, our neural recorder was able to extract signals from high impedance source while exhibiting up to an 18.5 dB lower system loss due to the high sensitivity of the circuit. Given that a minimum detectable power level is −130 dBm at the state-of-art spectrum analyzer, emulated neural

signals can be detected in frequency domain even it is as low as 47 μVpp from 20 Kohms source and 25 μVpp from 50 Ohms source.

(a)

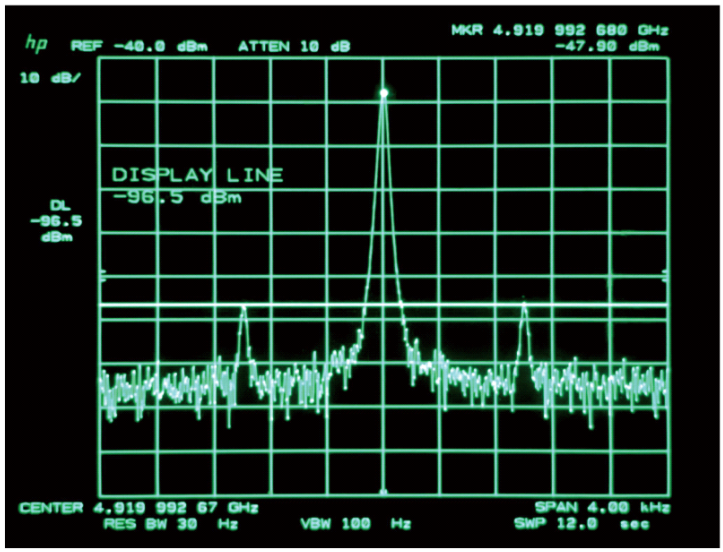

(b)

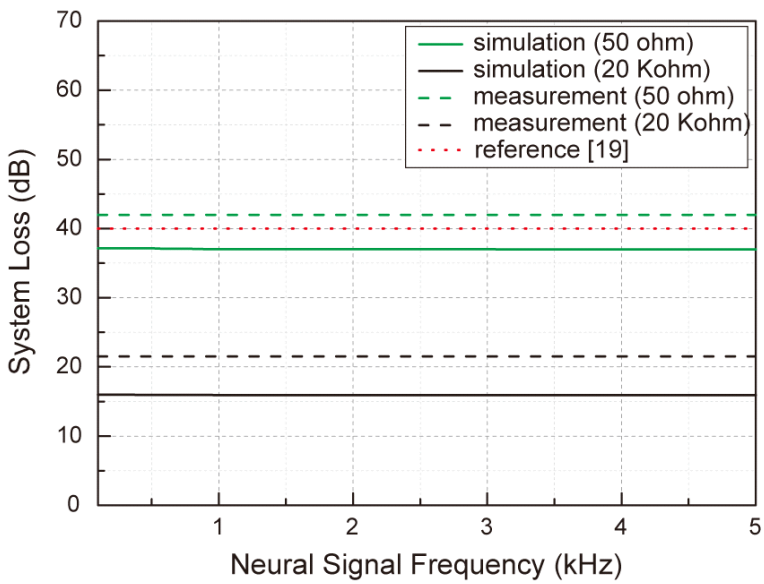

Figure 7 (a) Measured spectral response of a neural mote system to emulated neural signals (2 mV_{pp} at 1 kHz). (b) System loss as a function of neural signal frequency.

3.3. Time-domain performance

Also in the time domain, backscattering signal (4.92 GHz ± fneural) received from antenna was filtered, amplified, and demodulated in signal recovery block, and recovered neural potentials were shown through an oscilloscope. In this condition, a Minimum Detectable Signal at receiver (MDSRX) can be defined as

$$\begin{aligned} MDS_{\mathrm{RX}}\left[\mathrm{dBm}\right] &= kT\left(\mathrm{dBm/Hz}\right)+\log_{10}5\mathrm{kHz}+\mathrm{NF}+\mathrm{SNR} \\ &= -174+37+4+3=-130dBm \end{aligned} \tag{4}$$

where kT is the thermal noise level, NF is a noise figure of BJT and signal recovery block, and SNR is the minimum signal-to-noise ratio [19]. In this calculation, the value of NF is assumed to be a minimum level achievable with commercial filters and amplifiers to evaluate maximum performance of the mote. According to the equation (4) and (5), the neural mote can detect brain signals as low as 47 μ Vpp from 20 Kohms source and 25 μ Vpp from 50 Ohms source. The emulated neural signal recovery was demonstrated with 1 mVpp input waves (sine and extracellular potential) from 20 Kohms source, and the result of real-time signal recovery is shown in Fig. 5. (c) after post-digital filtering. As seen in Fig. 5. (c), characteristic sinusoidal waveforms were measured and recovered, and it was possible to detect evoked potential in time scale. On the top of that, superimposed data

in Fig. 5. (d) shows that waveform of the neural signal can be recovered without serious distortion due to the linear spectral response of the circuit. However, a relatively high level of noise was generated in the signal recovery block due to the high insertion loss of filter and the noise figure of amplifiers. Further improvement on the signal recovery block will be required to achieve the maximum performance of the implant.

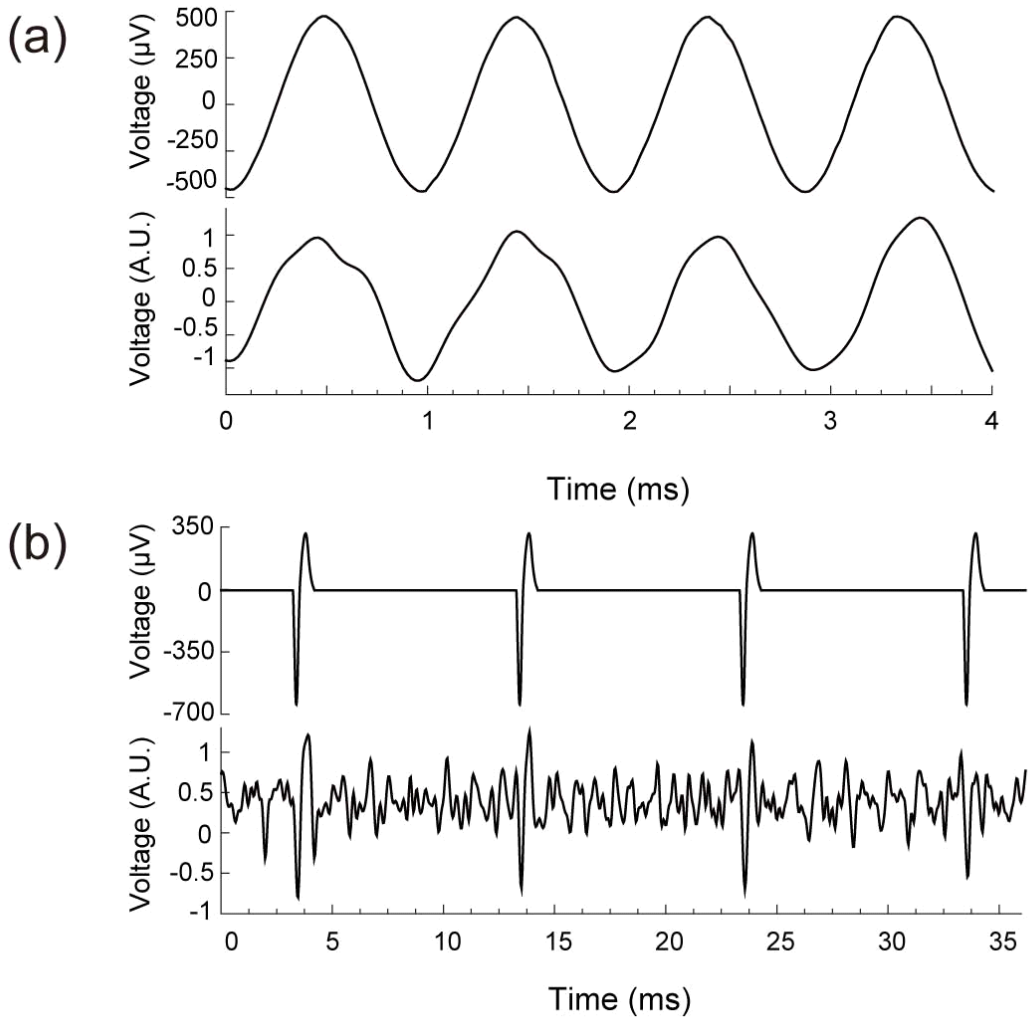

Figure 8 System loss as a function of neural signal frequency. (c) An example of input signals and recovered waveforms of sinusoid wave (left) and extracellular potential (right). The arbitrary function generator with 20 Kohm source impedance produced input signals of $1mV_{pp}$ at 1kHz.

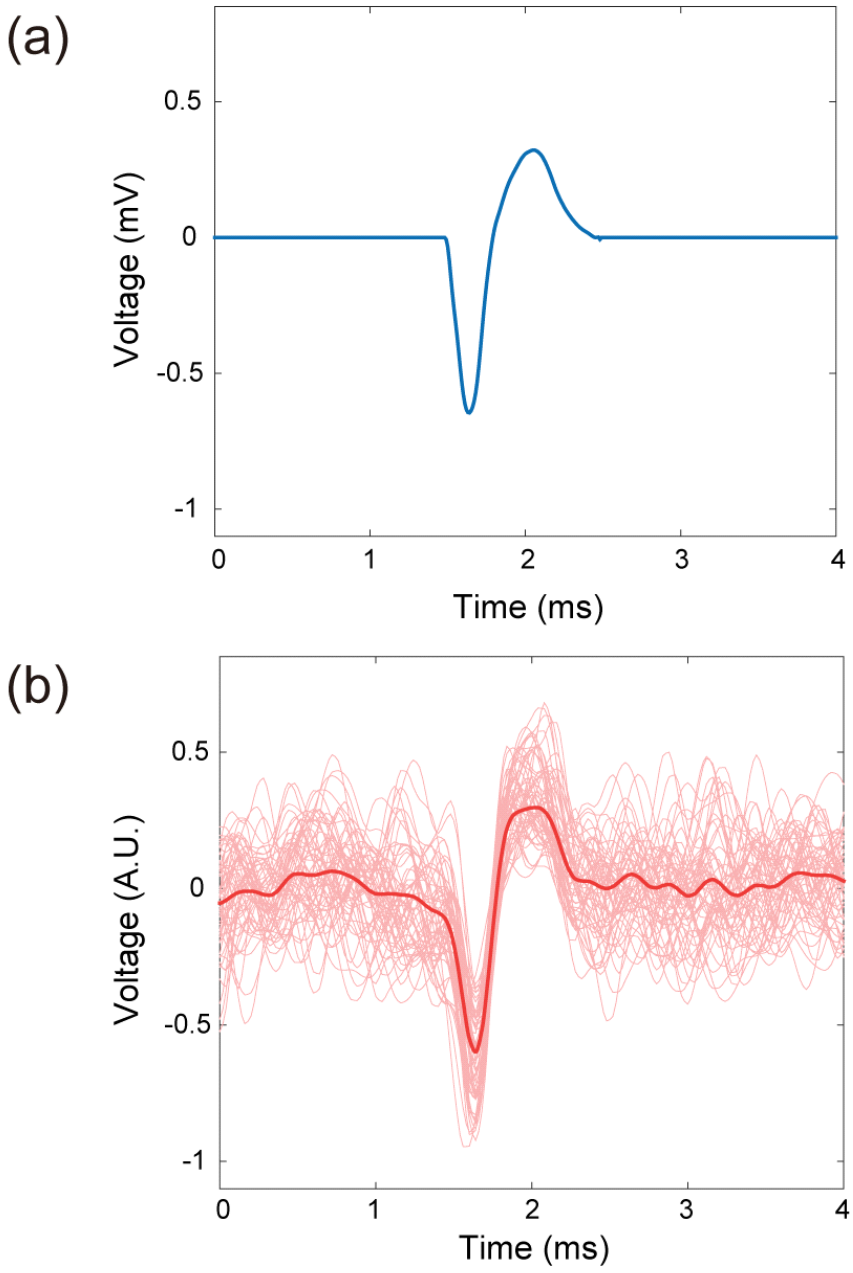

Figure 9 The input extracellular potential waveform (up) and the recovered signals (down) superimposed in a 4 ms window.

3.4. Specific Absorption Ratio (SAR) performance

The thermographic measurement shows that the linear correlation between the radiation time and the temperature rise of the tissue phantom having a coefficient of determination of 0.98486. This correlation implies that a thermal diffusion was negligible in this condition (see Fig. 6a). In resolving SAR at each pixel, slopes of the fitted trend-line between ΔT and Δt was calculated and multiplied by the heat capacity C (bone 1300 J/(kg•K) and other layers 3750 J/(kg• K)). Pixel SAR was averaged over 1g and 10g of tissue while assuming equal distribution along its orthogonal plane to estimate the maximum possible SAR [37]. Fig. 6 shows 1g-averaged SAR distribution, which rapidly decay away from the source antenna. At the source power of 1.58W, the maximum SAR10g value was measured as 31 W/kg comparable to the simulated value 30.32 W/kg. Therefore, according to the IEEE Safety guidelines [39], a source power meeting the maximum permitted level of exposure (10 W/kg) is 0.5 W (26.9 dBm). Considering the 5.5 dB higher system loss in measurement, this reduced level of power is sufficient to operate our system with improved matching condition. Future implementations will consider further reduction of the antenna's transmit power below this level to ensure the long-term safety of RF radiation.

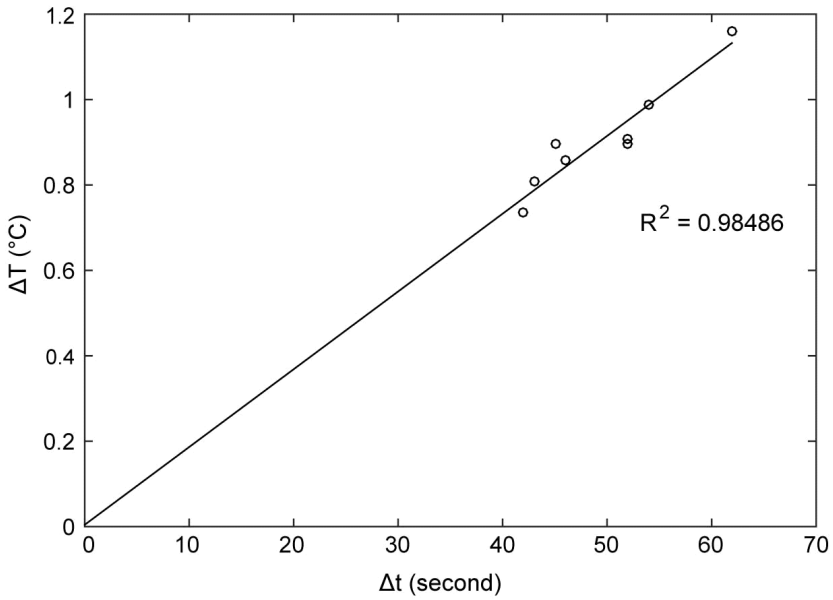

(a)

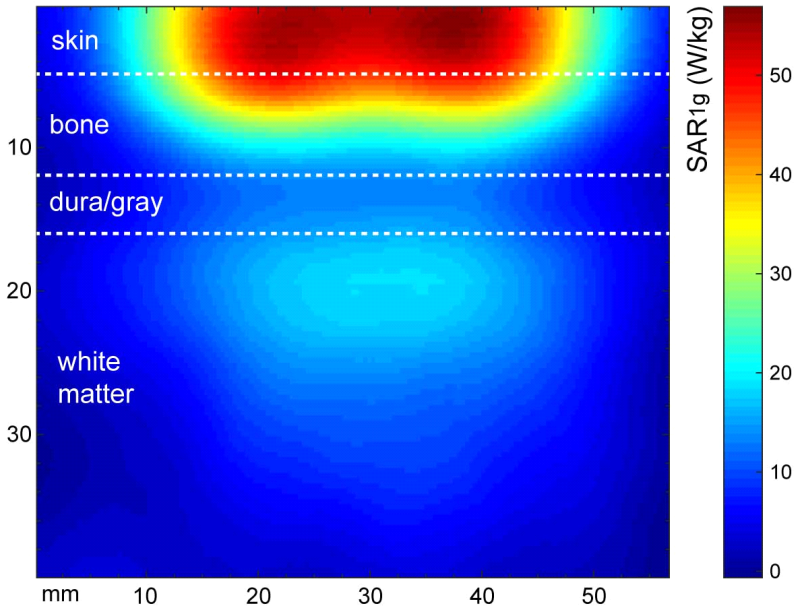

(b)

Figure 10 The result of SAR measurement (a) Temperature rise of phantom as a function of RF radiation exposure duration. (b) Spatial SAR_{1g} distribution measured using thermographic method.

Chapter 4. Conclusion

A highly efficient neural recording mote was suggested for an implantable brain-machine interface. This mote is only the size of a grain of rice (3 mm × 5 mm), which is only approximately 6% of that of a comparable passive neural implant. Even with this micro-miniaturized footprint, it can theoretically monitor extracellular potential levels as low as 47 μV_{pp} due to the high conversion gain (up to 17 dB) from the neural signals to the backscattered signals. This minimum detection level implies that this system can record the majority of the action potentials and the electrocorticographic signals from the brain [9, 39]. In addition, the implant circuit has the ability to extract signals from a high-impedance source (20 KOhms), which makes this system suitable for *in-vivo* recording conditions. To achieve these characteristics, our motes system employed 1) a novel dual-band midfield antenna for wireless powering and backscatter reading, and 2) a BJT RFID circuit for the nonlinear mixing of neural signals and carrier signals.

Due to its small footprint and passive operation, this system enables the minimally invasive monitoring of neural signals while mitigating the potential trauma or physiological interference caused by the implant. Thus, after an improvement of the long-term safety of the implant by reducing the transmit power and encapsulating the mote with biocompatible materials, our system can serve as a safe, portable,

and wearable BMI system. This system will be able to collect neural signals from subjects while allowing them to preserve their natural lifestyles and forgo extensive clinical care. Therefore, it can be used in a variety of clinical applications, such as for the early detection of epileptic seizures, the continuous monitoring of Alzheimer's disease, or control of neural prosthetics.

References

[1] A. V. Nurmikko, J. P. Donoghue, L. R. Hochberg, W. R. Patterson, Y. K. Song, C. W. Bull, D. A. Borton, F. Laiwalla, S. Park, Y. Ming, and J. Aceros, "Listening to Brain Microcircuits for Interfacing With External World-Progress in Wireless Implantable Microelectronic Neuroengineering Devices: Experimental systems are described for electrical recording in the brain using multiple microelectrodes and short range implantable or wearable broadcasting units," *Proc IEEE Inst Electr Electron Eng,* vol. 98, no. 3, pp. 375-388, 2010.

[2] L. R. Hochberg, D. Bacher, B. Jarosiewicz, N. Y. Masse, J. D. Simeral, J. Vogel, S. Haddadin, J. Liu, S. S. Cash, P. van der Smagt, and J. P. Donoghue, "Reach and grasp by people with tetraplegia using a neurally controlled robotic arm," *Nature,* vol. 485, no. 7398, pp. 372-U121, May 17, 2012.

[3] L. R. Hochberg, M. D. Serruya, G. M. Friehs, J. A. Mukand, M. Saleh, A. H. Caplan, A. Branner, D. Chen, R. D. Penn, and J. P. Donoghue, "Neuronal ensemble control of prosthetic devices by a human with tetraplegia," *Nature,* vol. 442, no. 7099, pp. 164-71, Jul 13, 2006.

[4] K. Sung-Phil, D. S. John, R. H. Leigh, P. D. John, and J. B. Michael, "Neural control of computer cursor velocity by decoding motor cortical spiking activity in humans with tetraplegia," *Journal of Neural Engineering,* vol. 5, no. 4, pp. 455, 2008.

[5] B. Jarosiewicz, A. A. Sarma, D. Bacher, N. Y. Masse, J. D. Simeral, B. Sorice, E. M. Oakley, C. Blabe, C. Pandarinath, V. Gilja, S. S. Cash, E. N. Eskandar, G. Friehs, J. M. Henderson, K. V. Shenoy, J. P. Donoghue, and L. R. Hochberg, "Virtual typing by people with tetraplegia using a self-calibrating intracortical brain-computer interface," *Sci Transl Med,* vol. 7, no. 313, pp. 313ra179, Nov 11, 2015.

[6] W. Truccolo, L. R. Hochberg, and J. P. Donoghue, "Collective dynamics in human and monkey sensorimotor cortex: predicting single neuron spikes," *Nat Neurosci,* vol. 13, no. 1, pp. 105-111, 01//print, 2010.

[7] X. Zou, L. Liu, J. H. Cheong, L. Yao, P. Li, M.-Y. Cheng, W. L. Goh, R. Rajkumar, G. S. Dawe, and K.-W. Cheng, "A 100-channel 1-mW implantable neural recording IC," *Circuits and Systems I: Regular Papers, IEEE Transactions on,* vol. 60, no. 10, pp. 2584-2596, 2013.

[8] J. Aceros, M. Yin, D. A. Borton, W. R. Patterson, and A. V. Nurmikko, "A 32-channel fully implantable wireless neurosensor for simultaneous recording from two cortical regions." pp. 2300-2306.

[9] R. R. Harrison, "The design of integrated circuits to observe brain activity," *Proceedings of the IEEE,* vol. 96, no. 7, pp. 1203-1216, 2008.

[10] Y.-K. Song, W. R. Patterson, C. W. Bull, J. Beals, N. Hwang, A. P. Deangelis, C. Lay, J. L. McKay, A. V. Nurmikko, and M. R. Fellows, "Development of a chipscale integrated microelectrode/microelectronic device for brain implantable neuroengineering applications," *IEEE transactions on neural systems and rehabilitation engineering,* vol. 13, no. 2, pp. 220-226, 2005.

[11] A. B. David, Y. Ming, A. Juan, and N. Arto, "An implantable wireless neural interface for recording cortical circuit dynamics in moving primates," *Journal of Neural Engineering,* vol. 10, no. 2, pp. 026010, 2013.

[12] Y. K. Song, D. A. Borton, S. Park, W. R. Patterson, C. W. Bull, F. Laiwalla, J. Mislow, J. D. Simeral, J. P. Donoghue, and A. V. Nurmikko,

"Active microelectronic neurosensor arrays for implantable brain communication interfaces," *IEEE Trans Neural Syst Rehabil Eng,* vol. 17, no. 4, pp. 339-45, Aug, 2009.
[13] C. A. Chestek, V. Gilja, P. Nuyujukian, S. I. Ryu, K. V. Shenoy, R. J. Kier, F. Solzbacher, and R. R. Harrison, "HermesC: RF wireless low-power neural recording system for freely behaving primates." pp. 1752-1755.
[14] S. Kim, P. Tathireddy, R. A. Normann, and F. Solzbacher, "In vitro and in vivo study of temperature increases in the brain due to a neural implant." pp. 163-166.
[15] M. L. Homer, A. V. Nurmikko, J. P. Donoghue, and L. R. Hochberg, "Implants and decoding for intracortical brain computer interfaces," *Annual review of biomedical engineering,* vol. 15, pp. 383, 2013.
[16] S. Kim, P. Tathireddy, R. A. Normann, and F. Solzbacher, "Thermal impact of an active 3-D microelectrode array implanted in the brain," *IEEE Transactions on Neural Systems and Rehabilitation Engineering,* vol. 15, no. 4, pp. 493-501, 2007.
[17] E. Moradi, S. Amendola, T. Bjorninen, L. Sydanheimo, J. M. Carmena, J. M. Rabaey, and L. Ukkonen, "Backscattering Neural Tags for Wireless Brain-Machine Interface Systems," *Antennas and Propagation, IEEE Transactions on,* vol. 63, no. 2, pp. 719-726, 2015.
[18] H. N. Schwerdt, F. A. Miranda, and J. Chae, "A Fully Passive Wireless Backscattering Neurorecording Microsystem Embedded in Dispersive Human-Head Phantom Medium," *Ieee Electron Device Letters,* vol. 33, no. 6, pp. 908-910, Jun, 2012.
[19] A. Kiourti, C. W. Lee, J. Chae, and J. L. Volakis, "A Wireless Fully Passive Neural Recording Device for Unobtrusive Neuropotential Monitoring," *IEEE Trans Biomed Eng,* vol. 63, no. 1, pp. 131-7, Jan, 2016.
[20] D. Seo, J. M. Carmena, J. M. Rabaey, M. M. Maharbiz, and E. Alon, "Model validation of untethered, ultrasonic neural dust motes for cortical recording," *J Neurosci Methods,* vol. 244, no. 0, pp. 114-22, Apr 15, 2015.
[21] H. N. Schwerdt, W. Xu, S. Shekhar, A. Abbaspour-Tamijani, B. C. Towe, F. A. Miranda, and J. Chae, "A fully passive wireless microsystem for recording of neuropotentials using RF backscattering methods," *Microelectromechanical Systems, Journal of,* vol. 20, no. 5, pp. 1119-1130, 2011.
[22] J. S. Ho, S. Kim, and A. S. Poon, "Midfield wireless powering for implantable systems," *Proceedings of the IEEE,* vol. 101, no. 6, pp. 1369-1378, 2013.
[23] J. Kim, and Y. Rahmat-Samii, "Implanted antennas inside a human body: Simulations, designs, and characterizations," *IEEE Transactions on microwave theory and techniques,* vol. 52, no. 8, pp. 1934-1943, 2004.
[24] S. Gabriel, R. W. Lau, and C. Gabriel, "The dielectric properties of biological tissues: II. Measurements in the frequency range 10 Hz to 20 GHz," *Phys Med Biol,* vol. 41, no. 11, pp. 2251-69, Nov, 1996.
[25] C. W. Lee, A. Kiourti, J. Chae, and J. L. Volakis, "A High-Sensitivity Fully Passive Neurosensing System for Wireless Brain Signal Monitoring," *Microwave Theory and Techniques, IEEE Transactions on,* vol. 63, no. 6, pp. 2060-2068, 2015.
[26] S. F. Cogan, "Neural stimulation and recording electrodes," *Annu. Rev. Biomed. Eng.,* vol. 10, pp. 275-309, 2008.

[27] G. Buzsáki, "Large-scale recording of neuronal ensembles," *Nature neuroscience,* vol. 7, no. 5, pp. 446-451, 2004.
[28] J. Lee, I. Ozden, Y. K. Song, and A. V. Nurmikko, "Transparent intracortical microprobe array for simultaneous spatiotemporal optical stimulation and multichannel electrical recording," *Nat Methods*, Oct 12, 2015.
[29] S. Kim, J. S. Ho, and A. S. Poon, "Midfield wireless powering of subwavelength autonomous devices," *Phys Rev Lett,* vol. 110, no. 20, pp. 203905, May 17, 2013.
[30] J. S. Ho, A. J. Yeh, E. Neofytou, S. Kim, Y. Tanabe, B. Patlolla, R. E. Beygui, and A. S. Poon, "Wireless power transfer to deep-tissue microimplants," *Proc Natl Acad Sci U S A,* vol. 111, no. 22, pp. 7974-9, Jun 3, 2014.
[31] S. Kim, J. S. Ho, and A. S. Poon, "Wireless power transfer to miniature implants: transmitter optimization," *Antennas and Propagation, IEEE Transactions on,* vol. 60, no. 10, pp. 4838-4845, 2012.
[32] J. M. C. Dongjin Seo, Jan M. Rabaey, Elad Alon, Michel M. Maharbiz, "Neural Dust: An Ultrasonic, Low Power Solution for Chronic Brain-Machine Interfaces," *eprint arXiv:1307.2196*, 2013.
[33] K. Ito, K. Furuya, Y. Okano, and L. Hamada, "Development and characteristics of a biological tissue-equivalent phantom for microwaves," *Electronics and Communications in Japan (Part I: Communications),* vol. 84, no. 4, pp. 67-77, 2001.
[34] Y. Okano, K. Ito, I. Ida, and M. Takahashi, "The SAR evaluation method by a combination of thermographic experiments and biological tissue-equivalent phantoms," *Microwave Theory and Techniques, IEEE Transactions on,* vol. 48, no. 11, pp. 2094-2103, 2000.
[35] H. N. Schwerdt, F. A. Miranda, and J. Chae, "Analysis of electromagnetic fields induced in operation of a wireless fully passive backscattering neurorecording microsystem in emulated human head tissue," *Microwave Theory and Techniques, IEEE Transactions on,* vol. 61, no. 5, pp. 2170-2176, 2013.
[36] "IEEE Recommended Practice for Determining the Peak Spatial-Average Specific Absorption Rate (SAR) in the Human Head from Wireless Communications Devices: Measurement Techniques," *IEEE Std 1528-2003*, pp. 1-120, 2003.
[37] H. N. Schwerdt, F. A. Miranda, and J. Chae, "Analysis of Electromagnetic Fields Induced in Operation of a Wireless Fully Passive Backscattering Neurorecording Microsystem in Emulated Human Head Tissue," *Ieee Transactions on Microwave Theory and Techniques,* vol. 61, no. 5, pp. 2170-2176, May, 2013.
[38] A. P. Chandrakasan, N. Verma, and D. C. Daly, "Ultralow-power electronics for biomedical applications," *Biomedical Engineering,* vol. 10, 2008.
[39] o. N.-I. R. H. IEEE Standards Coordinating Committee 28, *IEEE Standard for Safety Levels with Respect to Human Exposure to Radio Frequency Electromagnetic Fields, 3kHz to 300 GHz*: IEEE, 1992.
[40] G. Schalk, and E. C. Leuthardt, "Brain-computer interfaces using electrocorticographic signals," *IEEE reviews in biomedical engineering,* vol. 4, pp. 140-154, 2011.

요약(국문초록)

침습성 뇌-기계 인터페이스는 마비 및 뇌질환 환자의 운동이나 소통 능력을 보조할 수 있는 기술로 높은 임상적 가치를 갖는다고 여겨져 왔다. 그런데 현재까지의 시스템은 전극과 외부기기 간의 유선 연결을 요구하기 때문에 사용자의 외부감염 위험이 높고 행동적 제약이 크다. 이러한 문제점을 극복하기 위해 무선 뇌-기계 접속을 구현하려는 시도들이 있었으나 대부분 무선 임플란트의 크기가 크고 발열이 심하거나 외부전력 공급이 한정적이어서 이를 구성하는데 어려움이 있었다.

이에 본 연구는 중거리 무선 전력 전송 방법과 RFID(Radio-Frequency IDentification) 기술을 적용하여 높은 생체 안정성을 가진 초소형 무선 신경 임플란트 시스템을 구현하였으며 이를 적용하여 가상의 신경신호를 기록 및 추출하였다. 중거리 무선 전력 전송은 최적 전류 밀도를 통해 생체 내부에 높은 에너지 밀도 영역을 형성하는 방법으로 수신코일의 크기가 매우 작을 때도 많은 전력을 전달할 수 있다. 본 연구는 단일 위상 전력원을 통해서 최적 전류 밀도를 구현할 수 있는 중거리 무선전송 안테나를 설계 및 제작하였다. 안테나의 설계는 고주파 구조 해석을 통해 이루어졌고 2.46 GHz와 4.92 GHz 듀얼밴드에서 동작할 수 있도록 하여 높은 효율의 중거리 전력 송신과 RFID 데이터 수신을 구현하였다. 신경 임플란트는 상용소자를 이용해 구성하였는데 쇼트키 다이오드와 양극성 접합 트랜지스터로 구성된 패시브 RFID 센서로 제작하였다. 이 회로에서 쇼트키 다이오드는 수신된 2.46 GHz에서 4.92 GHz 고조파를 생성했고 트랜지스터는 비선형적 임피던스변화를 통해 4.92 GHz

반송파를 증폭된 신경신호로 변조시켰다. 상용소자는 집적 배열을 통해 직경 2mm 코일 내부에 실장하였고 전체적인 임플란트는 에폭시로 코팅하였다.

무선 전력공급 시스템과 임플란트의 동작검증은 생체와 유사한 유전율과 전기전도성을 가진 다층한천조직(피부, 두개골, 경막 및 회빌, 백질)에서 이루어졌으며 신경 임플란트를 두개골 아래에 이식하는 조건을 가정하였다. 이 때 신경 임플란트의 직경이 2mm에 불과할 때도 인체 전자파 노출 기준을 넘지 않으면서 수 mW의 전력을 전송할 수 있었고 수신된 전력을 이용해 신경신호가 담긴 3차 고조파가 생성됨을 확인하였다. 전극과 조직 사이의 임피던스가 수 십 Kohm일 때 변환 이득이 약 17 dB 정도 됨을 확인하였으며 이로 인해 100 μVpp 이하의 크기가 작은 신경신호까지 감지할 수 있었다. 또한 활동전위 주파수 범위 내에 선형성을 가지고 있어 외부에서 수신한 뒤 복조하였을 때 활동전위 파형을 왜곡 없이 추출할 수 있음을 검증하였다. 이는 기존의 RFID 신경센서 비해 10% 미만의 크기를 가지면서 높은 민감도를 갖는 신경 임플란트 시스템으로 무선 뇌-기계접속의 다양한 임상적인 적용 가능성을 시사한다.

……

주요어 : 뇌-기계 인터페이스, 중거리 무선 전력 전송, 신경 임플란트, 후방전송 센서, RFID(Radio-Frequency Identification)

학 번 : 2014-24817